Development and evaluation of a long range image-based monitoring system for civil engineering structures

Matthias Ehrhart*, Werner Lienhart

Institute of Engineering Geodesy and Measurement Systems, Graz University of Technology, Steyrergasse 30, 8010 Graz, Austria

ABSTRACT

Today, many large-scale civil engineering structures are permanently monitored to provide early warnings and to initiate counter actions from structural failure. Total station measurements are commonly used to determine 3D movements of selected points with measurement intervals of several minutes or hours. However, these measurements do not provide information on the vibration behavior of the structures. For this purpose, other sensors like accelerometers have to be installed on the object. In this paper, we present a monitoring system based on a state of the art image assisted total station (IATS) suitable for the measurement of absolute 3D coordinates and the determination of the structure's natural frequencies. The 3D coordinates can be determined with an accuracy of a few millimeters using conventional total station measurements. For analyzing the structure's natural frequencies, the telescope camera of the IATS is used in combination with dedicated image processing techniques optimized for artificial and natural targets. While the determination of 3D coordinates based on total station measurements is common practice, the idea of using the total station's image data for frequency analysis is new. Consequently, investigations on the achievable performance are pending for commercially available products. We therefore evaluate the potential of this technique at a life-size footbridge by comparison with accelerometer measurements. We demonstrate that with our developed monitoring concept and state of the art hardware, accelerometer measurements can be replaced in several monitoring situations by IATS measurements and image processing techniques.

Keywords: structural health monitoring, image assisted total station, telescope camera, pattern recognition, template matching, feature matching, optical flow

1. INTRODUCTION

Today, many large-scale civil engineering structures are permanently monitored to provide early warnings and to initiate counter actions from structural failure. This monitoring is commonly referred to as Structural Health Monitoring (SHM) and involves the investigation of the structure's vibration and displacement behavior. Vibration monitoring allows the identification of the structure's natural frequencies. This knowledge is important to initiate counter actions (e.g. integration of damping systems) to avert a structural failure if possible forced vibrations (caused by e.g. wind or traffic) are close to the natural frequencies[1],[2]. The displacement monitoring involves the long-term observation of the structure to investigate its movement due to diurnal (e.g. solar radiation) or annual (e.g. temperature variations) effects. It is also necessary for load testing which is done to validate the design of new bridges before they are approved for traffic[3].

Currently used measurement equipment for SHM involves accelerometers for vibration monitoring[1],[4],[5] and total stations[6],[7] or Global Navigation Satellite System (GNSS) instruments such as GPS receivers[8],[9],[10],[11] for displacement monitoring. Total stations and GNSS can also be used for vibration monitoring[8],[9],[12],[13],[14]. Although displacements can theoretically be computed by double-integration of accelerometer measurements over time, this does not work well in practice for long observation times and static loads[4],[8]. The currently used measurement equipment has the disadvantage that either the measurement sensors (for accelerometer and GNSS measurements) or special targets (for total station measurements) have to be attached to the monitored structure.

*matthias.ehrhart@tugraz.at; igms.tugraz.at

To overcome these limitations, different image-based approaches for vibration and displacement monitoring have been proposed[15],[16],[17],[18],[19]. To allow larger distances between the camera and the monitored structure, telescope lenses were used for the camera system[20],[21],[22]. These reported image-based systems use a single camera and are able to detect two-dimensional movements parallel to the sensor plane of the camera with up to 60fps[18],[19]. For the measurements it is sufficient to have simple target markings attached to the structure to be monitored. By using dedicated image processing techniques (e.g. template matching or optical flow), some systems do not require any artificial target markings at all[17]. However, these previously proposed methods have the common disadvantage that they require a stable point within the camera's field of view to control the stability of the setup. This is especially hard to establish for systems using telescope lenses due to their small field of view. Furthermore, the observed movements in the image (given in pixel) are related to units of length by comparison with a target of known size. This leads to systematic errors if the target is viewed from a skew angle which is not considered appropriately.

To overcome these problems we propose the use of total stations which are commonly utilized by surveyors to determine the 3D positions of targets. Modern total stations are equipped with a camera integrated in the telescope and are referred to as image assisted total stations (IATS). Currently, the camera is mainly used for documentation purposes but is a promising sensor for accurate measurements from long ranges since the angular resolution of the resulting image data benefits from the optical magnification of the telescope. The usage of IATS for vibration and displacement monitoring of civil engineering structures combines the advantages of conventional total station measurements (stability control) and image-based methods (simple or natural target markings). Furthermore, the observed pixel movements can be related to units of length by using the measured distance between the IATS and the monitored object. This makes the knowledge of the target size obsolete. The measured distance can also be used to automatically set the camera's focus position. Using IATS prototypes, experiments for the vibration monitoring of bridges were carried out[23],[24] whereat these approaches use active target markings requiring power supply.

We already reported on a novel approach to utilize a state of the art IATS for the vibration and displacement monitoring of civil engineering structures from long ranges using passive target markings[25]. In this paper, we introduce an extended version of our measurement system (Section 2) and describe our approach for the automated detection of the target markings (Section 3). We extend the original system[25] to allow the detection of natural targets (Section 3.2), examine the stability control of the camera (Section 4.1) and present additional measurement results based on artificial (Section 4.2) and natural (Section 4.3) targets. Finally, we discuss the suitability of the proposed system for practical measurement tasks (Section 5).

2. MEASUREMENT SYSTEM

2.1 Measurement sensor

The sensor of choice is the image assisted total station *MS50*[26] from *Leica Geosystems* (cf. Figure 1). A possible alternative to this instrument would be the IATS *Topcon IS-3*[27]. Conventional total station measurements are polar coordinates, i.e. the horizontal and vertical angles and the distance to a retro-reflective or a natural target. For the used instrument, the standard deviation of the angle measurements is specified with 1″. Electronic distance measurements (EDM) are possible up to 2000m where the standard deviation lies in the range of 1mm to 8mm dependent on the target type (retro-reflective/natural), the measurement mode (single/continuous) and the distance[26]. The Cartesian 3D coordinates of the sighted targets can be computed from the measured polar coordinates.

The key component for our studies is the total station's on-axis camera, i.e. a camera that is located in the optical path of the telescope. The images are captured by a 2560px × 1920px CMOS sensor. The camera has a 30x optical magnification resulting from the telescope and the field of view is specified with 1.5°[26]. The angular resolution of the camera was calibrated with 1.9630″/px in horizontal and vertical direction[25]. The live stream of the video data can be read with 10fps on an external computer where the frame size is reduced to 320px × 240px. Accordingly, reading the video stream of the camera's full field of view comprises a downsampling of the image data. Alternatively, a reduced field of view with full image resolution (one pixel in the image corresponds to one pixel on the CMOS sensor) can be used. To obtain high accurate measurement results, we decided to use the live stream at full image resolution and a reduced field of view.

Figure 1. MS50 total station from Leica Geosystems with camera located in the optical path of the telescope. The telescope axis coincides with the sighting axis (SA) of the total station. The telescope can be rotated about the vertical axis (VA) and the horizontal axis (HA). The measured quantities are the horizontal (Hz) and the vertical (V) angles and the distance (measured along SA) to a target.

Compared to a standard camera with telescope lenses, the usage of an IATS has several advantages. With the measured distance to the object it is possible to relate the angular quantities gained from image processing to units of length. Furthermore, the distance can be used to automatically set the telescope's focus motor position (autofocus). By reading the horizontal and vertical angles of the telescope and by monitoring the tilt of the instrument with the internal compensator, it is possible to control the instrument's stability during the recording of the image data. Another major advantage is the total station's ability to automatically rotate its telescope to predefined positions. It is generally possible to access all sensors of the total station (e.g. distance measurement unit, compensator, motorization, etc.) from an external computer via software commands using the GeoCOM[28] interface.

2.2 Measurement concept

The workflow of the measurements with our system is outlined in Figure 2. The whole process can be automated and several targets on different positions on the structure can be monitored sequentially. A user interaction is only required to initially sight the targets on the structure and to set the camera's recording properties. For long-term monitoring, where different targets are observed in regular intervals, a manual sighting is only necessary in the first measurement epoch. Afterwards, the stored positions are used to automatically rotate the total station's telescope to the corresponding targets.

The pixel movements between two frames i and j can either be computed relative to the first frame ($j = 1$) or between consecutive frames. The latter is not suited for displacement monitoring since the pixel movements relative to the first frame $\Delta x_{i,1}$ and $\Delta y_{i,1}$ have to be computed by cumulating the consecutive movements $\Delta x_{j+1,j}$ and $\Delta y_{j+1,j}$. This is unfavorable due to a propagation of random errors in the consecutive movements. For vibration monitoring, a conversion of the pixel movements to units of length is not necessary[25]. To eliminate trends in the time series prior to the computation of the frequencies via Fourier transformation, accelerations are computed from the pixel movements. Here, the usage of consecutive pixel movements is preferable to reduce noise in the resulting frequency spectrum. The accelerations $\ddot{x}_i$ and $\ddot{y}_i$ are computed from

$$\ddot{x}_i = \frac{\Delta x_{i+1,i} - \Delta x_{i,i-1}}{\Delta t^2} \ \text{ and } \ \ddot{y}_i = \frac{\Delta y_{i+1,i} - \Delta y_{i,i-1}}{\Delta t^2} \tag{1}$$

where the sampling rate Δt is 0.1s for a frame rate of 10fps. The subscript i denotes the frame position in the time series.
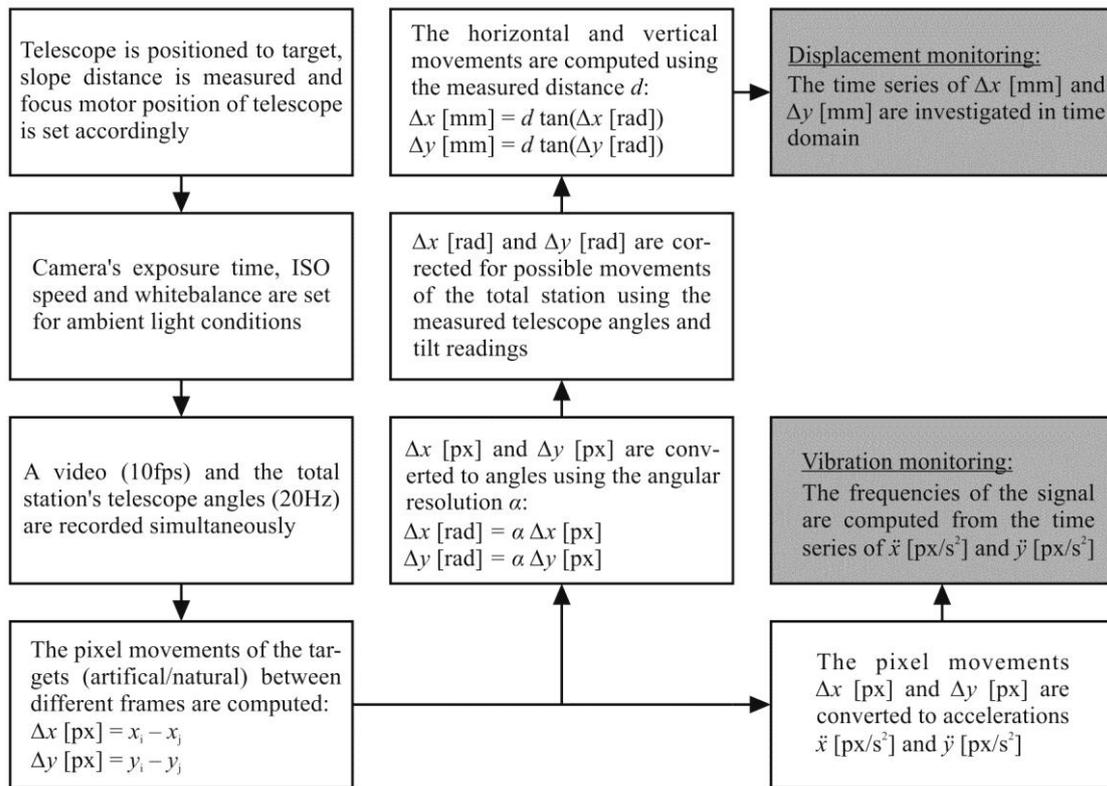
Figure 2. Workflow of the image-based measurement system for the determination of vibrations and displacements of moving structures.

For high accurate displacement monitoring, the measured displacements need to be corrected for possible rotations of the camera. Camera rotations can occur due to small, unintended rotations of the telescope or due to tilts of the whole total station. Both effects are measured by the total station (angle measurements and tilt readings). The correction is achieved by subtracting the camera rotations from the image-based angle measurements to the target. Prior to the correction, we smooth the camera rotation time series with a moving average filter[29] using an empirically determined filter length of 10s. This step is necessary to filter random noise in the total station's angle measurements and tilt readings.

With the proposed image-based measurements, the detection of object movements perpendicular to the total station's sighting axis is possible. To measure movements along the sighting axis, the total station's EDM can be used. For the monitoring applications described in this paper, only the angular resolution of the camera needs to be calibrated. This can be done with a fast and simple approach and without additional measurement equipment by using the total station's ability to automatically rotate its telescope to precisely known positions[25].

3. IMAGE PROCESSING

The measurement sensor of the proposed system is the total station's on-axis camera (cf. Section 2). Accordingly, image-based techniques have to be used to compute the positions (in pixel) of different targets on the camera's image sensor. The pixel movements are then processed according to Figure 2. The targets can be classified into artificial (Section 3.1) and natural (Section 3.2) targets where each group requires dedicated detection algorithms.

3.1 Artificial targets

The detection workflow for our passive, circular target markings (simple printouts) is outlined in Figure 3. We already reported on the procedure[25] but summarize the basic steps for the sake of completeness. The colored image is first con-

verted to an 8 bit grayscale image with pixel values between 0 (black) and 255 (white). Afterwards, a threshold is applied converting the grayscale image to a binary image, i.e. each pixel value below the threshold is set to 0 and each pixel value above the threshold is set to 1. Finally, the image coordinates of the marker's contour are computed by border following[30]. Based on the detected contours of the circle, its center coordinates including standard deviations are estimated by a least squares fit of an ellipse according to the Gauß-Helmert model[31],[32],[33].
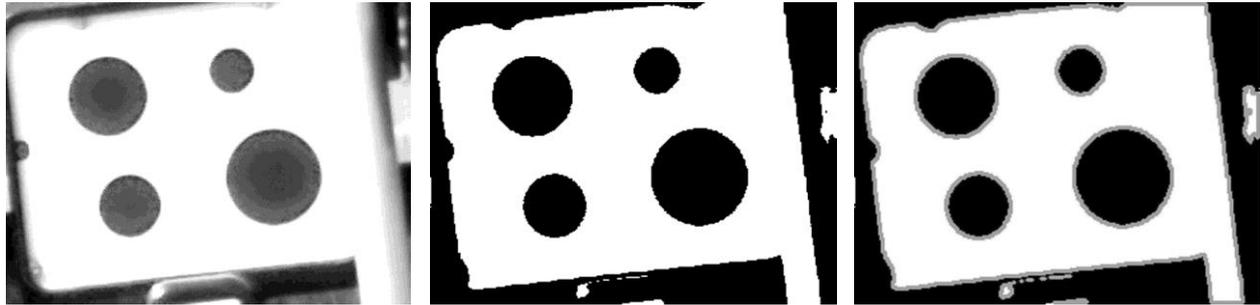
Figure 3. Illustration of the marker detection workflow with original frame (left), applied threshold (middle) and detected contours (right).

3.2 Natural targets

By using circular target markings, the proposed measurement system comprises the drawback that access to the monitored structure is necessary for attaching the targets. In cases of denied access due to e.g. safety regulations, omitting the artificial target markings is necessary. We evaluate the computation of the object movements from natural targets where three methods are investigated: template matching, feature matching and optical flow. Compared to previously reported vibration monitoring using a pure image-based system and natural targets[17], we extend the template matching approach to allow a sub-pixel detection of the object movements. Furthermore, we use more recent approaches for computing the optical flow between two images.

The generic workflow for detecting pixel movements from natural targets using the different processing methods is outlined in Figure 4. In a first common step, a region of interest (ROI) is selected in the captured image data (cf. Figure 5). The definition of this ROI is based on the assumption that all included pixel correspond to a rigid structure and have approximately the same distance to the total station. For the following processing steps, only the image data included in the ROI is considered. For all evaluated methods, the horizontal and vertical pixel movements of the ROI are computed between the actual frame and a reference frame. This reference frame may either be the first frame of the time series or the frame previous to the actual frame (cf. Section 2.2).
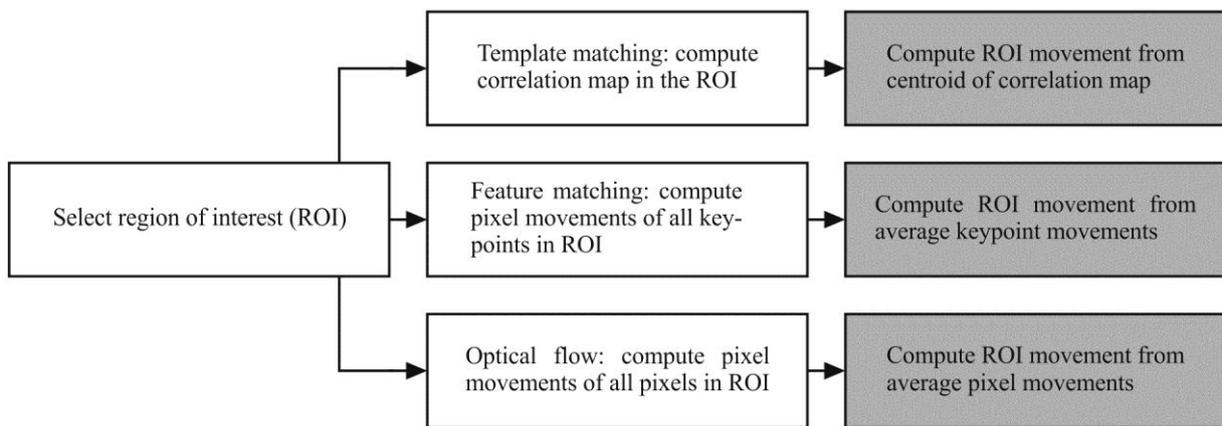
Figure 4. Illustration of possible workflows for computing pixel movements from natural targets.
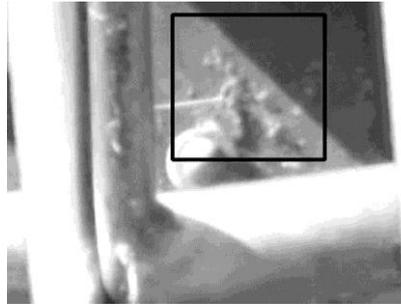
Figure 5. Selection of ROI (black rectangle) for image-based displacement and frequency monitoring with natural targets.

For the template matching approach, the correlation map with maximum values of 1 (perfect correlation) is computed between the actual frame and the reference frame. After applying an empirically determined threshold of 0.9, the weighted centroid of the resulting correlation map (cf. Figure 6, left) yields the pixel movements of the ROI between the two frames. For the weights, the values of the correlation map are used.

For the feature matching approach, keypoints of natural image features are detected in the actual and the reference frame (cf. Figure 6, middle). After computing the features' descriptors, corresponding keypoints in both frames are matched. The pixel movements of the ROI are computed as the average of all keypoint movements with previous outlier detection. For detecting and describing the image features, numerous methods have been proposed[34]. For our work, we decided to use the ORB[35] (Oriented FAST and Rotated BRIEF) method.

For the optical flow approach, the flow field between the actual frame and the reference frame is computed (cf. Figure 6, right). The pixel movements of the ROI are computed as the average of all pixel movements with previous outlier detection. For computing the optical flow between two images, several methods, dating back to the 1980ies[36],[37], have been proposed. For our work, we evaluated Farnebäck's algorithm[38] and the Dual TV L1 approach[39].

Figure 6. Different processing methods for computing pixel movements from natural targets. Left: template matching with correlation map. Middle: feature matching with detected keypoints. Right: optical flow with movements of selected pixel.

4. EXPERIMENTAL RESULTS

To assess the suitability of our system for practical measurements, we performed experiments at the Augarten footbridge in Graz, Austria. With the measurement configuration outlined in Figure 7 and the proposed image-based method (cf. Section 2.2), it is possible to measure vertical and lateral bridge movements. In this paper, we focus on the vertical movements. It is emphasized that our system is not limited to bridge monitoring but can also be employed for other civil engineering structures.
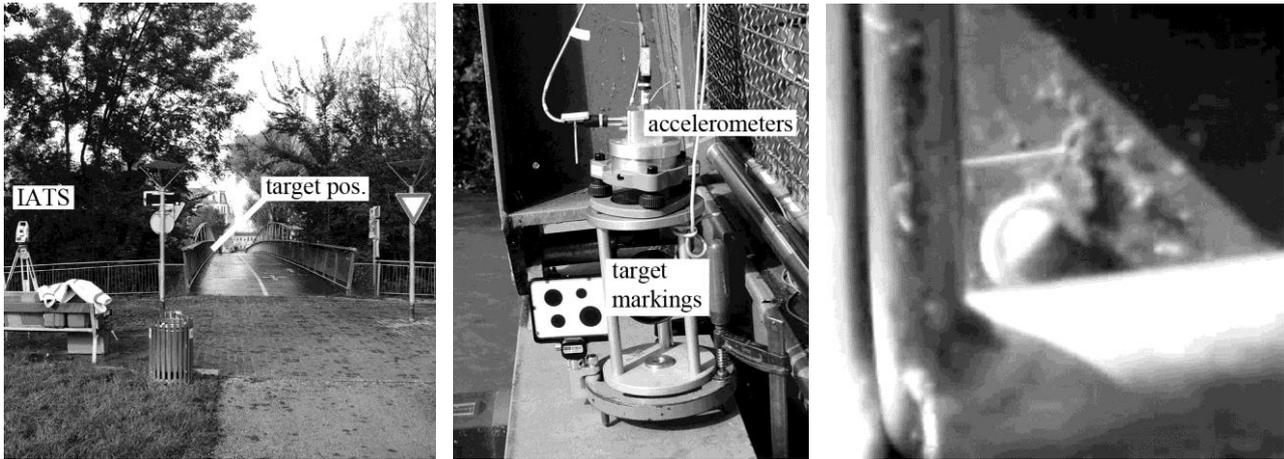
Figure 7. Augarten footbridge (left) equipped with passive target markings and accelerometers for reference measurements (middle) and natural targets (right).

4.1 Stability control

Figure 8 exemplarily depicts the vertical camera rotations and the heights measured by the IATS for a time period of 200s. The camera rotates in a range of ±1″ where the major contribution to the rotation is caused by variations in the tilt of the whole total station. For a distance of about 39m between the total station and the monitored object, a rotation of 1″ corresponds to an error of 0.2mm in the measured height. Accordingly, the heights need to be corrected for the camera rotation (cf. Section 2.2) to obtain high accurate results. For the depicted time series, an unconsidered camera rotation would mistake the trend (starting at time 50s) as an upward movement of the bridge deck (cf. Figure 8, middle and right).
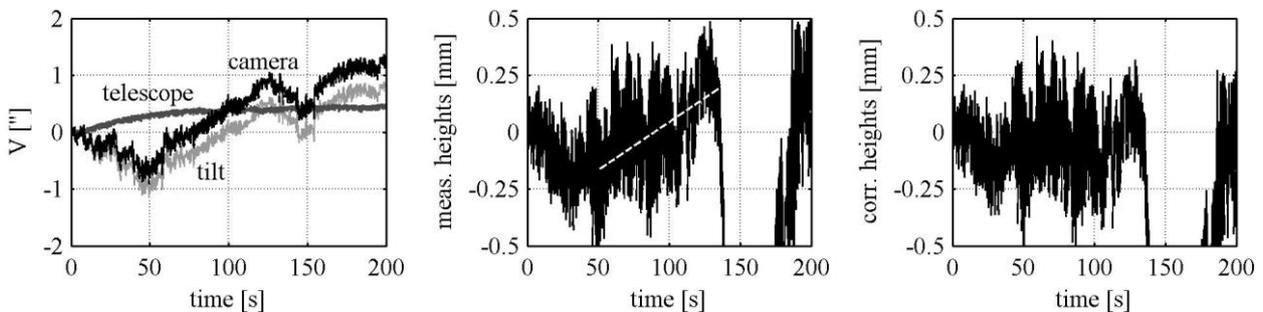
Figure 8. Vertical camera rotation resulting from the rotation of the telescope and the tilt of the total station (left). The measured heights with the apparent trend (middle) are corrected for the camera rotation to obtain corrected heights (right).

This experiment points out one advantage of an IATS over pure image-based systems with telescope lenses (cf. Section 1) which detect camera rotations from stable reference points. This approach for the stability control comprises the limitations that the stability of the reference point needs to be verified and that the reference point needs to be visible in the camera's field of view. The latter is hard to establish in practice due to the small field of view of cameras with telescope lenses.

4.2 Displacement and vibration monitoring

To assess the suitability of our system for practical measurements, we investigated the bridge's displacements and frequency responses for different loads and excitations. For reference measurements of the frequency responses, the bridge was equipped with an accelerometer HBM B12/200[40] oriented in vertical direction (cf. Figure 7). The distance between the total station and the circular target marking was about 39m. The scene observed by the IATS's camera is depicted in Figure 9 where we used the reduced field of view. The results presented below are based on the smallest target marking with a diameter of 15mm. The workflow of the measurements with the proposed system is outlined in Section 2.2.
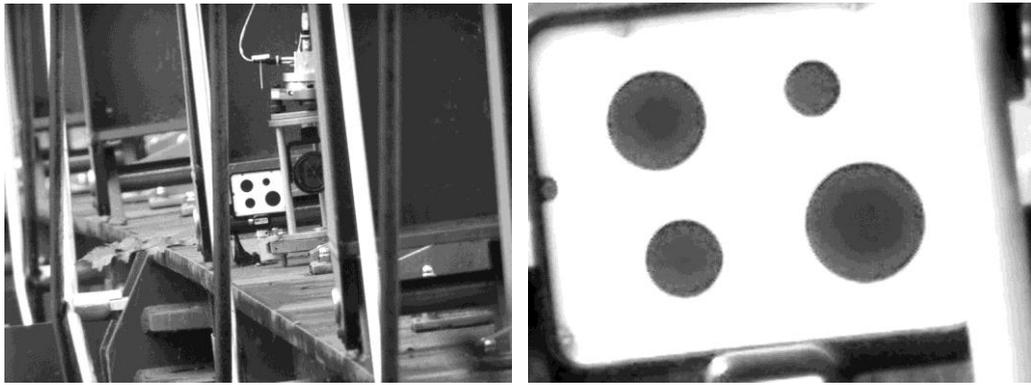
Figure 9. Complete (left) and reduced (right) field of view with circular target markings located at a distance of about 39m.

In laboratory experiments we showed that the circular target markings can be detected with a standard deviation of 0.3″ and that this value is roughly constant for different distances[25]. For the distance of 39m, 0.3″ translate to a standard deviation of 0.06mm for the detected movements. The temporal resolution for detecting the movements is 10Hz and results from the frame rate of the camera (10fps).

Figure 10 depicts the vertical displacements measured by the IATS and the measured reference accelerations caused by a vehicle driving over the bridge. From the displacement measurements, a maximum lowering of the bridge deck of about 2.5mm is visible. This maximum occurs when the vehicle is located in the central section of the bridge. This information cannot directly be derived from the accelerometer measurements.
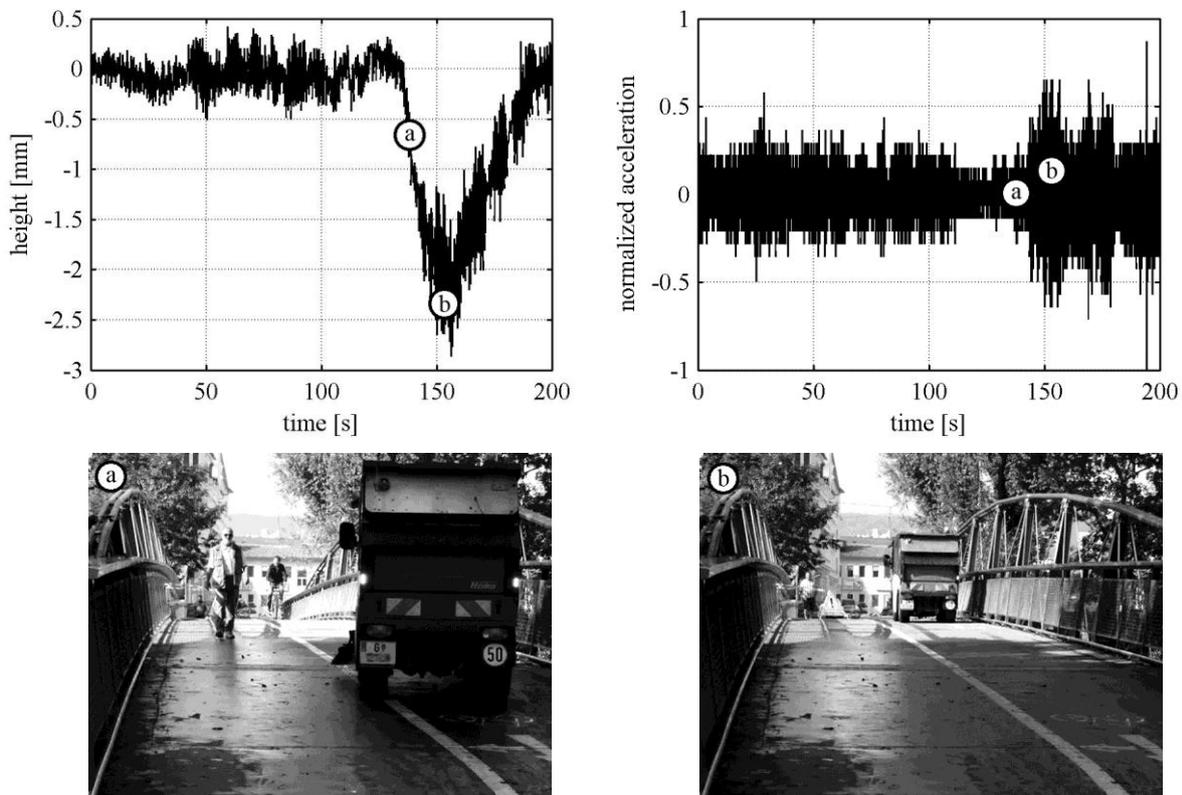
Figure 10. Height displacements measured with the IATS (top left) and vertical accelerometer measurements (top right) resulting from a vehicle driving over the bridge (bottom line).

Figure 11 depicts the frequencies included in the time series of Figure 10. For the dominant frequencies, the IATS measurements match the accelerometer measurements, which are conventionally used for vibration monitoring, almost perfectly. The frequencies in the range of $1.6 \text{Hz} < f < 2.1 \text{Hz}$ are probably caused by the different step frequencies of various walkers and runners crossing the bridge. A deeper investigating of the forces causing the frequencies is beyond the scope of this paper.
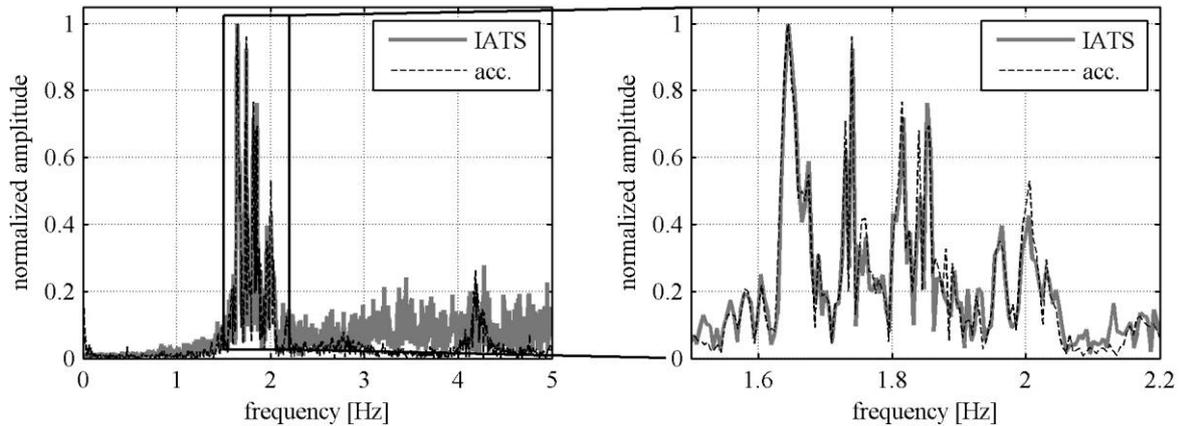
Figure 11. Amplitude spectral densities computed from IATS and accelerometer measurements resulting from a vehicle driving over the bridge. Left: complete spectrum. Right: detail with dominant frequencies.

Figure 12 depicts a displacement and acceleration time series resulting from a single runner passing the bridge and from a simultaneous crossing of a runner and a walker. Both time series reveal that a walker causes larger oscillations than a runner. However, the movements of the bridge deck can only be directly investigated from the IATS measurements where vertical displacements of ±1mm can be detected.

The frequency responses of the time series highlighted in Figure 12 are depicted in Figure 13. For the runner time series, the noise in the spectrum resulting from the IATS measurements is higher compared to the spectrum of the accelerometer measurements. However, the dominant frequency, which is the step frequency of the runner, can be identified from the IATS (2.86Hz) and the accelerometer (2.87Hz) measurements. For the spectrum resulting from a simultaneous crossing of a runner and a walker, the dominant frequency is 1.75Hz (IATS) and 1.74Hz (accelerometer). The magnitude of the bridge deck's oscillation rapidly increases when excited by a walker (cf. Figure 12). It can thus be concluded that the detected frequency of about 1.7Hz is close to the natural frequency of the bridge[2]. The signal component at 2.85Hz (IATS) and 2.84Hz (accelerometer) corresponds to the runner who was the same as for the runner time series.
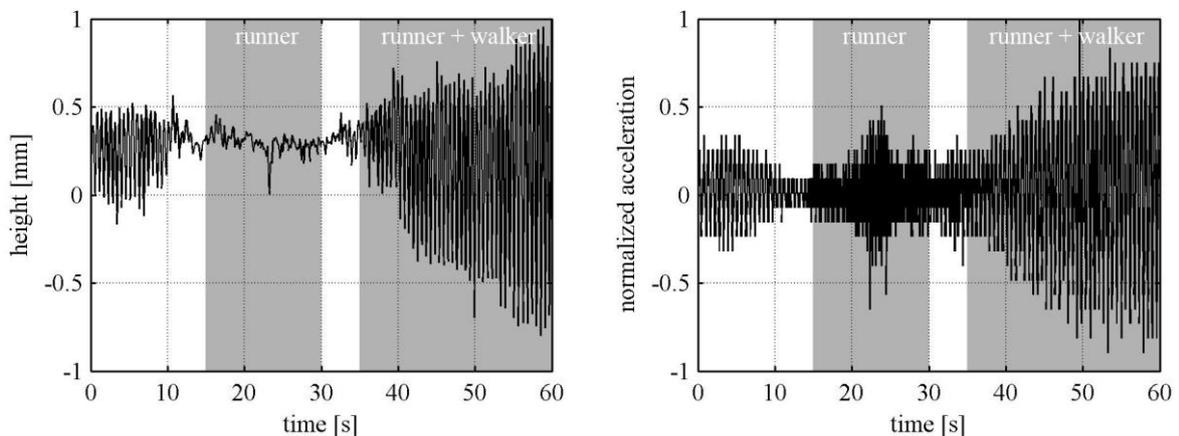
Figure 12. Height displacements measured with the IATS (left) and vertical accelerometer measurements (right) resulting from a single runner (left gray area) and from a simultaneous crossing of a runner and a walker (right gray area).
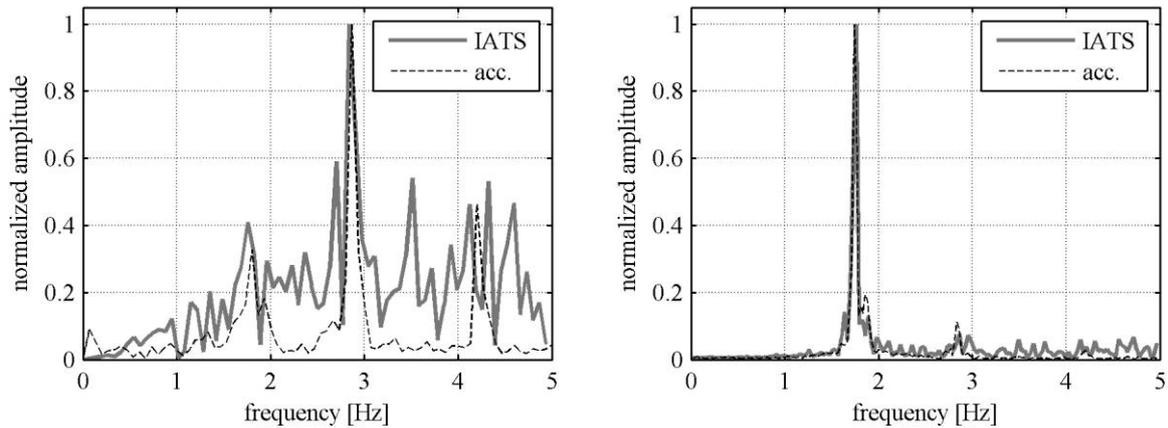
Figure 13. Amplitude spectral densities computed from IATS and accelerometer measurements resulting from a single runner (left) and from a simultaneous crossing of a runner and a walker (right).

4.3 Measurements with natural targets

In certain monitoring situations, access to the observed structure is not possible. We therefore evaluated the feasibility of replacing the artificial targets, which need access for attaching them, by natural targets included in the monitored structure. The distance between the total station and the natural targets was about 57m. The scene observed by the IATS's camera is depicted in Figure 14 where we used the reduced field of view. The workflow of the measurements with the proposed system is outlined in Section 2.2. The evaluated approaches for detecting movements from natural targets are described in Section 3.2.

Figure 14. Complete (left) and reduced (right) field of view for natural targets located at a distance of about 57m.

Figure 15 depicts the frequency responses computed from the IATS measurements and different methods for processing the natural targets. The measurements were carried out for 35s while the bridge was excited by runners and walkers. The different processing methods yield similar results where the prominent frequencies vary by less than 0.05Hz. The dominant frequency of 1.74Hz probably corresponds to the bridge's natural frequency and the signal component of 2.87Hz is due to the step frequency of the runner. This is in correspondence to the results determined with artificial targets markings and accelerometer measurements (cf. Section 4.2). The source for the frequency of 4.20Hz is not further investigated but it is mentioned that this signal was also detected in other experiments (cf. Figure 11 and Figure 13).
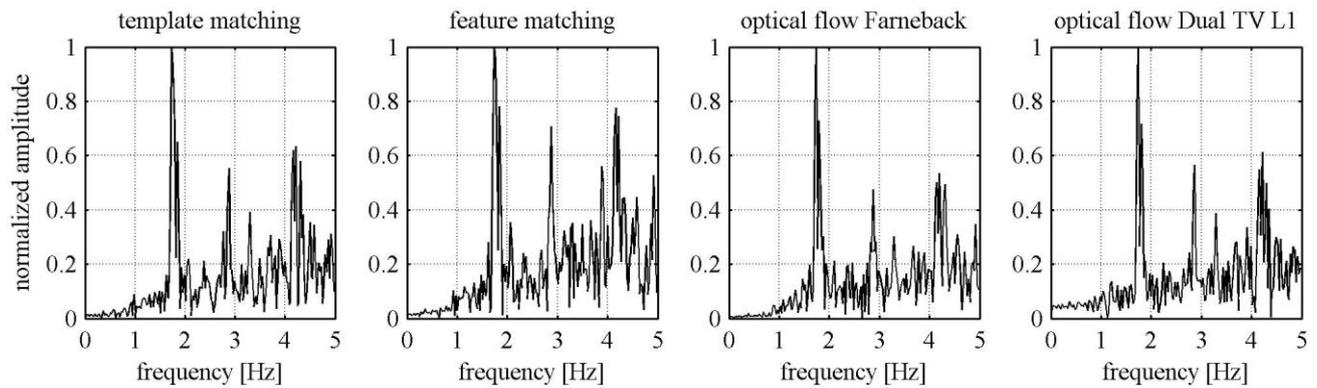
Figure 15. Amplitude spectral densities computed from IATS measurements and different methods for processing the natural targets.

Comparing the results to Section 4.2 demonstrates that it is possible to replace artificial target markings by using natural targets included in the monitored structure. For optical flow methods, the relative movement between two frames is computed from a plurality of individual pixel displacements (cf. Section 3.2). By computing the standard deviation of the individual displacements it is possible to exclude uncertain detections from further processing. It is furthermore possible to automatically select a ROI corresponding to a rigid structure (cf. Section 3.2) by investigating the directions and magnitudes in the flow field. We therefore recommend an optical flow method for the processing of natural targets.

5. CONCLUSIONS

In this paper, we reported on the vibration and displacement monitoring of civil engineering structures using a state of the art image assisted total station (IATS) and different target types. The core element of our measurements system is the total station's on-axis camera with an angular resolution of approximately $2''$ and a maximum frame rate of 10fps. The standard deviation for detecting a passive, circular target marking in a single frame is $0.3''$[25]. By using the total station's angle measurements and tilt readings, it is possible to verify the stability of the camera during the measurements and to apply corrections if necessary.

In a field experiment at a life-size footbridge and by comparison with accelerometer measurements, we demonstrated that the IATS is able to correctly identify the frequencies included in a civil engineering structure's oscillation. The proposed system can therefore replace accelerometer measurements in many cases. Accelerometer measurements are traditionally used for vibration monitoring and require access to the monitored structure and space for setting up the accelerometers including a data processing unit and power supply. By using natural targets instead of artificial target markings, no access to the monitored structure is necessary. This overcomes the problems arising for accelerometer measurements at civil engineering structures with limited access e.g. due to safety regulations.

The usage of natural targets is especially appealing in combination with ambient vibration monitoring where the structure is excited by natural forces such as wind[5]. With this strategy it is neither necessary to attach measurement sensors to the structure nor to excite the structure with dedicated devices[1]. With the proposed system it is furthermore possible to combine conventional total station measurements for displacement monitoring and accelerometer measurements for vibration analysis. Thus, only one measurement system with unified processing software is needed.

The shortcoming of the proposed measurement system is its recording frequency of 10Hz when transmitting the total station's live stream to an external computer. For the monitoring of bridges, frequencies of up to 20Hz are of interest[1],[5] and can be detected using an IATS prototype with frame rates up to 200Hz[24]. However, the critical natural frequencies of footbridges in vertical direction are only between 1.25Hz and 4.6Hz[1] and therefore can already be identified with the used state of the art IATS. Furthermore, manufacturers of IATS are currently recognizing the potential of image-based measurements with their instruments. Accordingly, the maximum frame rate might be improved for new generations of IATS.

REFERENCES

[1] Heinemeyer, C., Butz, C., Keil, A., Schlaich, M., Goldack, A., Trometer, S., Lukić, M., Chabrolin, B., Lemaire, A., Martin, P. O., Cunha, A. and Caetano, E., "Design of Lightweight Footbridges for Human Induced Vibrations", European Commission - JRC Scientific and Technical Reports, JRC 53442, EUR 23984 EN (2009).

[2] Dukkipati, R. V. and Srinivas, J., [Textbook of mechanical vibrations], 2nd ed., 6th print., PHI Learning, New Delhi (2012).

[3] The Institution of Civil Engineers, [Guidelines for the Supplementary Load Testing of Bridges], Thomas Telford Publications, London (1998).

[4] Faulkner, B. C., Barton, F. W., Baber, T. T. and McKeel, W. T., "Determination of bridge response using acceleration data", Report No. FHWA/VA-97-R5, Virginia Department of Transportation (1996).

[5] Wenzel, H. and Pichler, D., [Ambient Vibration Monitoring], John Wiley & Sons, West Sussex, England (2005).

[6] Radovanovic, R. S. and Teskey, W. F., "Dynamic monitoring of deforming structures: GPS versus robotic tacheometry systems", Proc. 10th FIG Symposium on Deformation Measurements, Orange, California, USA, 61-70 (2001).

[7] Kuhlmann, H. and Gläser, A., "Investigation of new Measurement Techniques for Bridge Monitoring", Proc. 2nd Symposium on Geodesy for Geotechnical and Structural Engineering, Berlin, Germany, 123-132 (2002).

[8] Celebi, M., "GPS in dynamic monitoring of long-period structures", Soil Dynamics and Earthquake Engineering 20, 477-483 (2000).

[9] Nakamura, S., "GPS Measurement of Wind-Induced Suspension Bridge Girder Displacements", Journal of Structural Engineering 126(12), 1413-1419 (2000).

[10] Wieser, A. and Brunner, F. K., "Analysis of Bridge Deformations using Continuous GPS Measurements", Proc. 2nd Conf. of Engineering Surveying, Bratislava, Slovakia (2002).

[11] Im, S., Hurlebaus, S. and Kang, Y., "Summary Review of GPS Technology for Structural Health Monitoring", Journal of Structural Engineering 139(10), 1653-1664 (2013).

[12] Cosser, E., Roberts, G. W., Meng, X. and Dodson, A. H., "Measuring the dynamic deformation of bridges using a total station", Proc. 11th FIG Symposium on Deformation Measurements, Santorini, Greece (2003).

[13] Lekidis, V., Tsakiri, M., Makra, K., Karakostas, C., Klimis, N. and Sous, I., "Evaluation of dynamic response and local soil effects of the Evripos cable-stayed bridge using multi-sensor monitoring systems", Engineering Geology 79(1-2), 43-59 (2005).

[14] Psimoulis, P. A. and Stiros, S. C., "Measurement of deflections and of oscillation frequencies of engineering structures using Robotic Theodolites (RTS)", Engineering Structures 29(12), 3312-3324 (2007).

[15] Wahbeh, A. M., Caffrey, J. P. and Masri, S. F., "A vision-based approach for the direct measurement of displacements in vibrating systems", Smart Materials and Structures 12(5), 785-794 (2003).

[16] Schwarz, W., "Vermessungen im Sub-Millimeter-Bereich", Allgemeine Vermessungs-Nachrichten 8-9, 341-350, (2007).

[17] Caetano, E., Silva, S. and Bateira, J., "A vision system for vibration monitoring of civil engineering structures", Experimental Techniques 35(4), 74-82 (2011).

[18] Choi, H. S., Cheung, J. H., Kim, S. H. and Ahn, J. H., "Structural dynamic displacement vision system using digital image processing", NDT&E International 44(7), 597-609 (2011).

[19] Kim, S. W. and Kim, N. S., "Multi-point Displacement Response Measurement of Civil Infrastructures Using Digital Image Processing", Procedia Engineering 14, 195-203 (2011).

[20] Olaszek, P., "Investigation of the dynamic characteristic of bridge structures using a computer vision method", Measurement 25(3), 227-236 (1999).

[21] Lee, J. J. and Shinozuka, M., "Real-Time Displacement Measurement of a Flexible Bridge Using Digital Image Processing Techniques", Experimental Mechanics 46, 105-114 (2006).

[22] Martins, L. L., Rebordão, J. M. and Ribeiro, A. S., "Conception and development of an optical methodology applied to long-distance measurement of suspension bridges dynamic displacement", Journal of Physics: Conference Series 459 (2013).

[23] Bürki, B., Guillaume, S., Sorber, P. and Oesch, H.P., "DAEDALUS: A Versatile Usable Digital Clip-on Measuring System for Total Stations", Proc. 2010 Intl. Conf. on Indoor Positioning and Indoor Navigation (IPIN), Zurich, Switzerland (2010).

[24] Wagner, A., Wasmeier, P., Reith, C., Wunderlich, T., "Bridge Monitoring by Means of Video-Tacheometer - A Case Study", Allgemeine Vermessungs-Nachrichten 8-9, 283-292 (2013).

[25] Ehrhart, M. and Lienhart, W., "Image-based dynamic deformation monitoring of civil engineering structures from long ranges", Proc. SPIE 9405 (2015).

[26] Leica Geosystems AG, "Leica MS50/TS50/TM50 User Manual", Version 1.1.1 (2013).

[27] Topcon Corp., "Imaging Station Instruction Manual" (2011).

[28] Leica Geosystems AG, "Leica Nova MS50 GeoCOM Reference Manual", Version 5.50 (2014).

[29] Brand, S., [Data analysis], 3rd ed., Springer, New York (1999).

[30] Suzuki, S. and Abe, K., "Topological Structural Analysis of Digitized Binary Images by Border Following", Computer Vision, Graphics, and Image Processing 30, 32-46 (1985).

[31] Grafarend E. W., [Linear and nonlinear models: fixed effects, random effects, and mixed models], de Gruyter, Berlin (2006).

[32] Niemeier, W., [Ausgleichungsrechnung], 2. Auflage, de Gruyter, Berlin (2008).

[33] Lenzmann, L. and Lenzmann, E., "Strenge Auswertung des nichtlinearen Gauß-Helmert-Modells", Allgemeine Vermessungs-Nachrichten 2, 68-73 (2004).

[34] Miksik, O. and Mikolajczyk, K., "Evaluation of local detectors and descriptors for fast feature matching", 21st Intl. Conf. on Pattern Recognition (ICPR), Tsukuba, Japan, 2681-2684 (2012).

[35] Rublee, E., Rabaud, V., Konolige, K. and Bradski, G., "ORB: An efficient alternative to SIFT or SURF", Proc. IEEE Intl. Conf. on Computer Vision, 2564-2571 (2011).

[36] Lucas, B. D. and Kanade, T., "An Iterative Image Registration Technique with an Application to Stereo Vision", Proc. 7th Intl. Joint Conf. on Artificial Intelligence (IJCAI), Vancouver, Canada, 674-679 (1981).

[37] Horn, B. K. P. and Schunck, B. G., "Determining Optical Flow", Artificial Intelligence 17, 185-203 (1981).

[38] Farnebäck, G., "Two-Frame Motion Estimation Based on Polynomial Expansion", Lecture Notes in Computer Science 2749, 363-370 (2003).

[39] Zach, C., Pock, T. and Bischof, H., "A Duality Based Approach for Realtime TV-L1 Optical Flow", Proc. 29th DAGM Symposium on Pattern Recognition, Heidelberg, Germany, 214-223 (2007).

[40] HBM Mess- und Systemtechnik GmbH, "Acceleration Transducer B12 Mounting Instructions", Version 17.2.2000 (2000).